A microchanneled ceramic membrane for highly-efficient oxygen separation

Xin Shao, Dehua Dong*, Gordon Parkinson and Chun-Zhu Li

Experimental details:

Membrane preparation and characterization: The ceramic membranes were prepared by a modified phase inversion process with subsequent sintering. Typically, 4.3 g of Polyethersulfone (PESF) and 0.7 g of Polyvinylpyrrolidone (PVP, MW=40000) were dissolved in 30 g of 1-Methyl-2-pyrrolidinone (NMP, 99%) in a beaker by magnetic stirring (chemicals were purchased from Sigma-Aldrich Australia). Then, 65 g of $La_{0.6}Sr_{0.4}Co_{0.2}Fe_{0.8}O_{3-\delta}$ (LSCF-6428, Fuel Cell Materials, USA) powder with a BET surface area of 5.5 cm^2/g was mixed with the above solution in a Teflon jar. The mixture was ball milled for 48 hours by a planetry ball-miller (MTI Corporation, USA) at a speed of 300 RPM to form a homogeneous slurry. Next, 0.4 ml of the prepared slurry was transfered into an aluminium mould by a syringe. After degassing, a stainless steel mesh was immersed just below the slurry surface. 5 ml of tap water was poured on top of the slurry to induce phase inversion for 20 min. Finally, the stainless steel mesh was gently lifted off from the solidified slurry. After drying at 80 °C for 60 min, the membrane was heated in a box furnace (ModuTemp Pty. Ltd., Australia) at 600 °C for 1 h to remove organic components and then sintered in air at 1350 °C for 5 h. The microstructure of the prepared membranes was observed by SEMs (Zeiss Neon 40EsB FIBSEM and Zeiss Evo 40XVP), and the mesh images were observed by a optical microscopy (Nikon Eclipss, ME600). Porosity was tested by a Archimedes‘ method. Three-point bending strength was measured on bar-shape membranes by a materials testing instrument (ZE50, Lloyd Instruments), and calculated according to the following equation:

$$\delta = \frac{3\mathrm{FL}}{2bh^2}$$

Where δ is the bending strength, MPa; F is the fracture load, N; L is the span length, mm; b and h are the width and height of the bar sample, mm.

Oxygen permeation test: To test oxygen permeation, the disc membrane was seated on a quartz tube by using ceramic adhesive (552-VFG, Aremco Products Inc., USA) as a sealant. The effective areas of the tested membranes are about 0.7 cm^2. The test was performed in a tubular furnace. Argon was used as a sweep gas, and air was used as a feed gas on the other side of the membrane with a constant flow rate of 270 ml min^{-1} in this experiment. The oxygen concentration in the sweep gas was measured by online gas chromatography (GC, GC-2014, Shimadzu) with a packed column of molecular sieve 5A, and the oxygen permeation flux was calculated using the following equation.

$$J_{O_2} = \frac{\mathrm{J}_{Sweep}(C_{O_2} - C_{N_2} * \frac{21}{79})}{\mathrm{A}}$$

where J_{O_2} is oxygen permeation flux, J_{Sweep} is the flow rate of sweep gas, C_{O_2} is the concentration of permeated oxygen in sweep gas and A is the effective permeation area of membrane. The thicknesses of all membranes were in the range of 0.80-0.85 mm. Oxygen leakage from the test system was below 1%, which was measured by the detected nitrogen levels.

Supporting experimental data

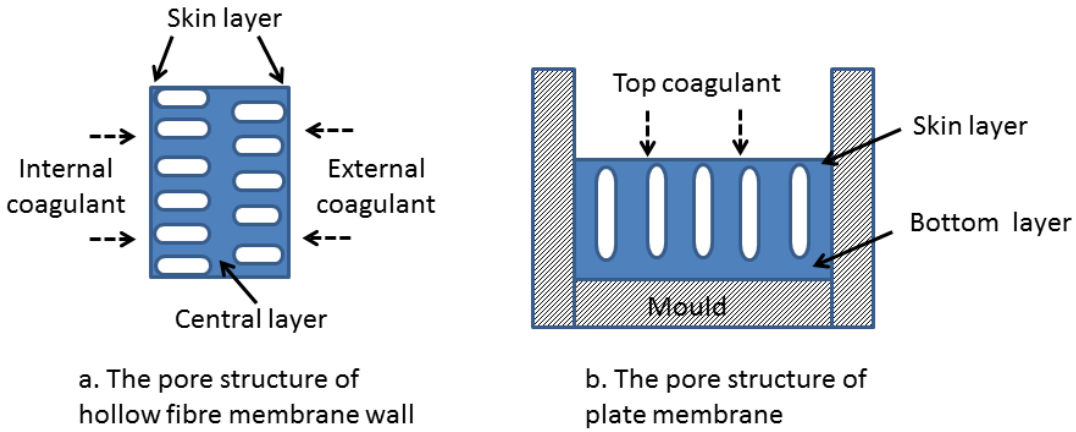

Fig. S1. Structure comparison of hollow fibre membranes and plate membranes prepared by phase inversion processes

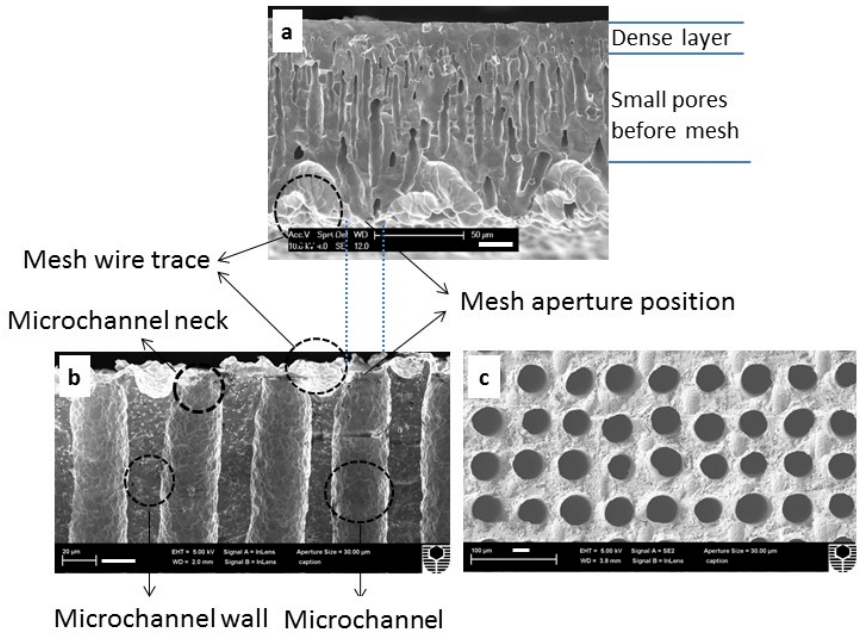

Fig. S2. SEM images of the cross section of the skin layer removed from the microchanneled membranes by a mesh (a), the top of microchanneled membrane (b) and the membrane surface after polishing away the neck part (c). Scale bar is 20 μm. As shown in the skin layer removed by lifting off the mesh, below a dense layer of about 15 μm in thickness, there are many small pore channels before the mesh wire trace. They start combining or disappearing

when they approach the mesh, and finally are forced into large pores channel by the mesh, templating microcahnnels.

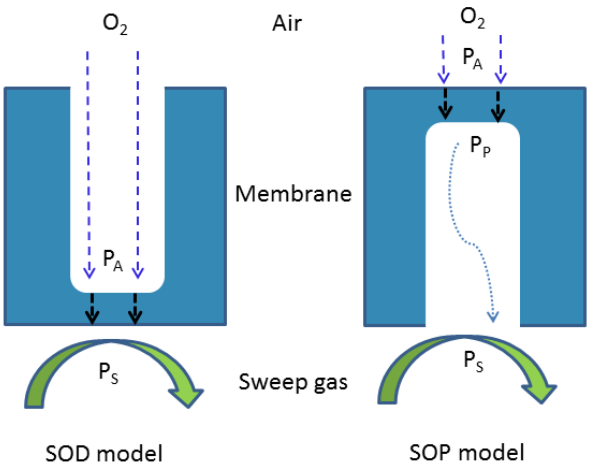

Fig. S3. Schematic representation of different test models of oxygen permeation through the microchanneled membrane.

According to Wagner‘s equation:

$$J_{O_2} = \frac{\delta_e \delta_i}{16F^2 L(\delta_e + \delta_i)} \ln\left(\frac{P'_{o_2,feed}}{P''_{o_2},sweep}\right)$$

The OPF is determined by oxygen partial pressures on the feed gas side and the sweep gas side. For the feed gas side, both models have the same oxygen partial pressure P_A considering the high concentration of oxygen in air and low oxygen permeation fluxs. On the contrary, for the sweep gas side the oxygen partial pressure within micochannels (P_P) for the SOP model is higher than the oxygen partial pressure in the sweep gas (P_S) for the SOD model due to diffusion resistance within the micro-channels, i.e. $P_P > P_S$. Accordingly, P_A/P_P is smaller than P_A/P_s. The OPF in SOP model is determined by P_A/P_P while the OPF in SOD model is determined by P_A/P_s. Therefore, the OPFs for the SOD model are higher than that for the SOP model.

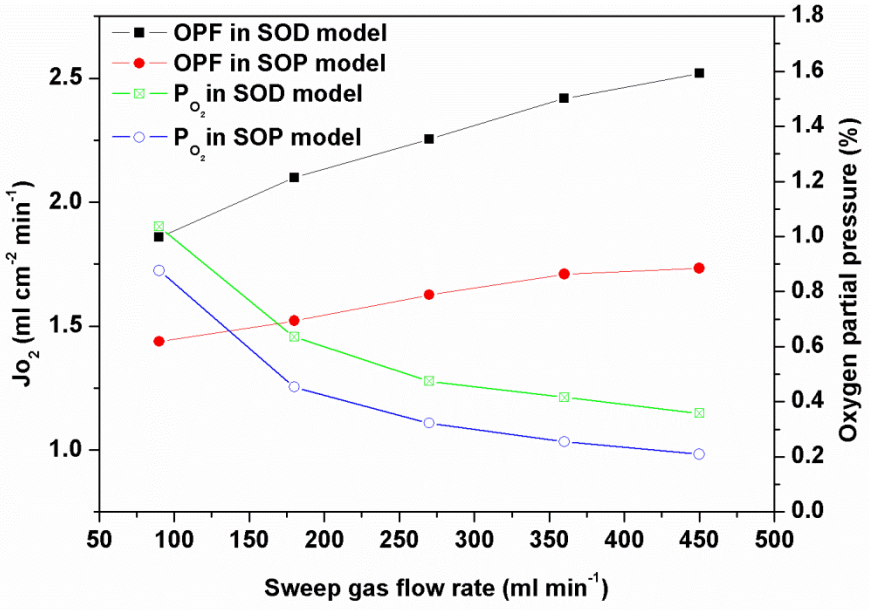

Fig. S4. The effects of sweep gas flow rate on the OPF at 1000 °C and oxygen partial pressure on sweep side tested under the SOP model and SOD model on the microchanneled membrane.

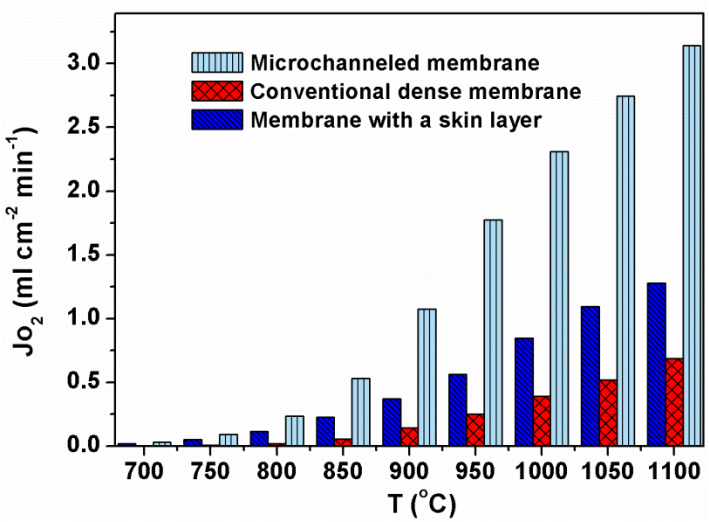

Fig. S5. The OPF comparison of different membranes in this study.

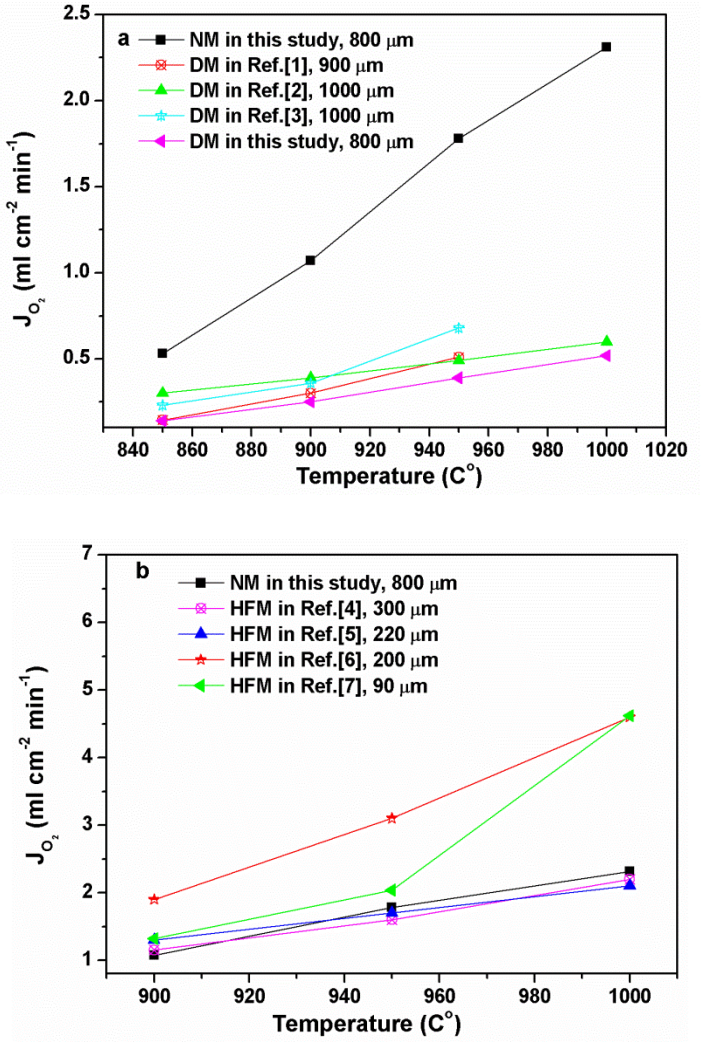

Fig. S6. The OPF comparisons of the new membrane (NM) developed in this study with (a) conventional dense membranes (DM)[1-3] and (b) hollow fibre membranes (HFM).[4-7] The thicknesses of membranes were indicated in the figure.

To our knowledge, the figure includes the highest OPFs of LSCF-6428 membranes reported in the literature, and the thicknesses of the membranes are also shown. The new membrane produced much higher OPFs than those reported for conventional dense membranes. The oxygen permeation performances are even comparable with those of hollow fibre membranes with wall thicknesses of 250-300 μm, and are only lower than those of ultra-thin hollow fibre membranes (100-200 μm). However, the practical application of hollow fibres with a wall thickness less than 300 μm may be limited as a result of the reduced mechanical strength.

1. Y. Zou, W. Zhou, S. M. Liu and Z. P. Shao, *J. Eur. Ceram. Soc.*, **2011**, 31, 2931-2938.

2. A. A. Asadi, A. Behrouzifar, M. Iravaninia, T. Mohammadi and A. Pak, *Ind. Eng. Chem. Res.*, **2012**, 51, 3069-3080.

3. P. Y. Zeng, R. Ran, Z. H. Chen, H. X. Gu, Z. P. Shao, J. C. D. da Costa and S. M. Liu, *J. Membr. Sci.,* **2007**, 302, 171-179.

4. X. Y. Tan, Z. G. Wang and K. Li, *Ind. Eng. Chem. Res.,* **2010**, 49, 2895-2901.

5. Z. G. Wang, H. Liu, X. Y. Tan, Y. G. Jin and S. M. Liu, *J. Membr. Sci.*, **2009**, 345, 65-73.

6. N. Liu, X. Y. Tan, B. Meng and S. M. Liu, *Sep. Purif. Technol.*, **2011**, 80, 396-401.

7. B. Zydorczak, Z. T. Wu and K. Li, *Chem. Eng. Sci*., **2009**, 64, 4383-4388.